Neuro-Oncology
26(5), 811–825, 2024 | https://doi.org/10.1093/neuonc/noad214 | Advance Access date 6 November 2023

TREM2 mediates MHCII-associated CD4$^+$ T-cell response against gliomas

Jiaying Zheng, Lingxiao Wang, Shunyi Zhao, Wenjing Zhang, Yuzhou Chang, Dale B. Bosco, Tao Huang, Aastha Dheer, Shan Gao, Shengze Xu, Katayoun Ayasoufi, Rawan Al-Kharboosh, Fangfang Qi, Manling Xie, Aaron J. Johnson, Haidong Dong, Alfredo Quiñones-Hinojosa, and Long-Jun Wu

All author affiliations are listed at the end of the article

Corresponding Author: Long-Jun Wu, PhD, Department of Neurology, Mayo Clinic, 200 First Street SW, Rochester, MN 55905, USA (Wu.Longjun@mayo.edu).

Abstract

Background. Myeloid cells comprise up to 50% of the total tumor mass in glioblastoma (GBM) and have been implicated in promoting tumor progression and immunosuppression. Modulating the response of myeloid cells to the tumor has emerged as a promising new approach for cancer treatment. In this regard, we focus on the Triggering Receptor Expressed on Myeloid Cells 2 (TREM2), which has recently emerged as a novel immune modulator in peripheral tumors.

Methods. We studied the TREM2 expression profile in various patient tumor samples and conducted single-cell transcriptomic analysis in both GBM patients and the GL261 mouse glioma model. We utilized multiple mouse glioma models and employed state-of-the-art techniques such as *in vivo* 2-photon imaging, spectrum flow cytometry, and *in vitro* co-culture assays to study TREM2 function in myeloid cell-mediated phagocytosis of tumor cells, antigen presentation, and response of CD4$^+$ T cells within the tumor hemispheres.

Results. Our research revealed significantly elevated levels of TREM2 expression in brain tumors compared to other types of tumors in patients. TREM2 was predominantly localized in tumor-associated myeloid cells and was highly expressed in nearly all microglia, as well as various subtypes of macrophages. Surprisingly, in preclinical glioma models, TREM2 deficiency did not confer a beneficial effect; instead, it accelerated glioma progression. Through detailed investigations, we determined that TREM2 deficiency impaired the ability of tumor-myeloid cells to phagocytose tumor cells and led to reduced expression of MHCII. This deficiency further significantly decreased the presence of CD4$^+$ T cells within the tumor hemispheres.

Conclusions. Our study unveiled a previously unrecognized protective role of tumor-myeloid TREM2. Specifically, we found that TREM2 enhances the phagocytosis of tumor cells and promotes an immune response by facilitating MHCII-associated CD4$^+$ T-cell responses against gliomas.

Key Points

- In human gliomas, Triggering Receptor Expressed on Myeloid Cells 2 (TREM2) is correlated with phagocytosis and MHC Class II antigen presentation.
- Deficiency of TREM2 has no beneficial effect in preclinical models of glioma.
- TREM2 deficiency impairs myeloid cell phagocytosis of tumor debris.
- TREM2 deficiency leads to a reduction in MHCII-associated CD4$^+$ anti-glioma immunity.

Importance of the Study

Triggering Receptor Expressed on Myeloid Cells 2 (TREM2) has predominantly been recognized for its protective effects in neurodegeneration; however, recent studies have highlighted its role as a biomarker for tumor-associated myeloid cells and its detrimental impacts on peripheral tumor progression. The specific function of TREM2 in brain tumors remains largely unknown. Our study shows that, in contrast to peripheral tumors, TREM2 deficiency aggravates glioma progression. Our results further underscore the significance of myeloid TREM2 in promoting MHCII-associated CD4$^+$ T-cell responses in gliomas. Considering that TREM2 antagonists are emerging as potential therapeutic targets for cancer treatment, it is imperative to fully comprehend the diverse range of TREM2 functions in different immune cell types and carefully evaluate their influence on tumor progression.

Antitumor immunity requires the presence of both major histocompatibility complex (MHC) class I and MHC Class II,[1] which activate CD8$^+$ and CD4$^+$ cells, respectively, although their tumoricidal contributions vary across different types of tumors. For instance, in murine colon adenocarcinoma and sarcomas, antitumor immunity relies on CD8$^+$ T-cell infiltration and effectively responds to anti-programmed cell death protein 1 (PD-1) immunotherapy.[2–4] In contrast, in brain tumors, recent studies have suggested that MHC Class II-restricted CD4$^+$ tumor-infiltrating T cells play a key role in regulating tumor clearance.[5,6] As a result, anti-cytotoxic T-Lymphocyte-associated Antigen 4 (CTLA4), but not anti-PD-1, extended the survival of glioma mice in a CD4$^+$ T-cell-dependent manner.[5]

MHC Class II-restricted antigen presentation requires antigen-presenting cells to efficiently engulf and degrade exogenous antigenic material.[7] As a cell surface receptor, Triggering Receptor Expressed on Myeloid Cells 2 (TREM2) is expressed exclusively in microglia[8] in the central nervous system (CNS), macrophages,[9] and dendritic cells.[10,11] The deficiency of TREM2 impairs the ability of microglia to sense and degrade numerous antigenic materials, including but not limited to pathogens,[12] apoptotic neurons,[13] β-amyloid,[14–16] TAR DNA binding protein 43 (TDP-43),[17] myelin,[18] and neuronal synapses.[19] Early studies reported that upon ligation of TREM2, genes related to MHC Class II rapidly upregulate.[10] Additionally, tumor-myeloid cells in CD4$^+$ mediated glioma regression upregulated genes involved in pathways related to phagocytosis, including *Trem2*.[5] Increased phagocytosis of tumor cells by macrophages has been shown to prolong the survival of glioma-burden mice.[20]

Interestingly, TREM2 deficiency reduced the immunosuppression of tumor-associated myeloid cells, suggesting that TREM2 can be detrimental in mouse models of peripheral tumors.[3,4,21–23] Here, we found that brain tumors exhibited significantly higher levels of *TREM2* expression compared to the paired normal tissues, predominantly in tumor-associated myeloid cells. TREM2 was not correlated with immunosuppressive markers but correlated with genes associated with phagocytosis and MHC Class II antigen presentation. Consistently, TREM2 deficiency in classic glioma murine models did not slow disease progression. We further revealed that loss of TREM2 dampened the ability of myeloid cells to phagocytose tumor cells and express MHC Class II. Our study highlighted the importance of myeloid TREM2 in promoting MHCII-associated CD4$^+$T-cell response in gliomas.

Materials and Methods

Animals

The *Trem2*$^{-/-}$ line was kindly provided by Dr. Marco Colonna at Washington University School of Medicine, St. Louis, and was bred at Mayo Clinic.[17] Wild-type mouse line was purchased from Jackson Laboratory. All animals were housed under standard conditions (21°C–22°C; 55% humidity) in individually ventilated cages, with a 12-h light/dark cycle and ad libitum access to food and water. Male and female mice aged between 8 and 14 weeks were used in the studies. All experimental procedures were approved by the Mayo Clinic's Institutional Animal Care and Use Committee (IACUC).

Tumor Cell Culture

Murine GL261 glioma inoculation of C57BL/6 mice is a well-established experimental model of human glioblastoma (GBM).[24] GL261 is a syngeneic mouse model of GBM in C57BL/6 mice that does not require an immunodeficient host.[25] The GL261 cell line transduced with firefly luciferase (GL261-luc) for *in vivo* monitoring of tumor kinetics was kindly provided by the laboratory of Dr. Aaron J. Johnson (Mayo Clinic, Rochester, MN, USA). The cell line GL261-luc transduced with mCherry (GL261-luc-mCherry) for an *in vivo* phagocytosis study was generated by the laboratory of Dr. Alfredo Quiñones-Hinojosa (Mayo Clinic, Jacksonville, FL, USA). Cells were grown in Dulbecco's modified Eagle medium (DMEM; Gibco, #11965092) with 10% fetal bovine serum (FBS; Sigma-Aldrich, #F2442) and 1% Penicillin-Streptomycin (Gibco, # 15140122), in a 37°C humidified incubator with 5% CO_2. For tumor inoculation, cells were dissociated with TrypLE Express (Gibco, # 12605010) and resuspended in phosphate-buffered saline (PBS) at a final concentration of 5×10^4 cells per μL.

The murine 73C glioma model utilizes astrocyte-derived gliomas harboring *p53*$^{-/-}$, *Pten*$^{-/-}$, and *Braf*^{V600E} mutations, leading to the formation of intracranial tumors consistent with high-grade histopathology.[26,27] The cell line was kindly provided by the laboratory of Dr. Woo-ping Ge (University of Texas Southwestern Medical Center, Dallas, TX, USA). For tumor inoculation, cells were dissociated with TrypLE

Express and resuspended in PBS at a final concentration of 1×10^4 cells per μL.

The murine MC38 cell line derived from C57BL6 murine colon adenocarcinoma[28] was kindly provided by the laboratory of Dr. Haidong Dong (Mayo Clinic, Rochester, MN, USA). Cells were grown in Roswell Park Memorial Institute Medium (RPMI; Corning, #10-040-CV) with 10% FBS and 1% PenicillinStreptomycin, in a 37°C humidified incubator with 5% CO_2. For tumor inoculation, cells were dissociated with TrypLE Express, washed and resuspended in PBS at a final concentration of 5×10^3 cells per μL.

Inoculation of GL261 and 73C Glioma Cells

Under isoflurane anesthesia, a 0.5-cm longitudinal incision was made on the scalp, and a burr hole was drilled using a high-speed dental drill (ML: ±1.5; AP: +1.5). Using a stereotactic frame, the needle of a Hamilton syringe was then lowered 3.5 mm into the striatum and a total of 5×10^4 GL261-luc cells in 1–2 μL were injected, as previously described.[29] Similarly, for 73C inoculation, a total of 1×10^4 cells in 1–2 μL were injected. The wound was closed using 6-0 ETHILON Nylon Suture (Ethicon, #1660G).

To assess tumor burden in GL261-luc-bearing mice, bioluminescence imaging was used as previously described.[29] Mice were intraperitoneally (IP) injected with 200 μL of 15 mg/μL D-Luciferin in PBS (Goldbio, #LUCK-1G), and anaesthetized with 2% isoflurane during imaging. Mice were scanned using the IVIS Spectrum system (Xenogen Corp.) at Mayo Clinic, running Living Image software.

To evaluate the tumor burden in mice bearing the 73C glioma, the mouse brains were dissected, and the tumor weight was calculated by subtracting the weight of the contralateral hemisphere from that of the tumor hemisphere.

For the survival study, the mice were closely monitored, and when they reached a humane endpoint, showing signs such as hunching, bulging head, or weight loss of approximately 20%, they were euthanized. Additionally, the survival of WT mice with 5×10^4 GL261 tumor cell inoculation consistently remains around 4 weeks, which has been set as a reliable control for experiments.

Inoculation of MC38 Tumor Cells

MC38 cells were washed, and resuspended in sterile PBS, and then injected subcutaneously into previously shaved flanks of the mice. A total of 5×10^5 cells in 100 μL PBS were injected into the mammary fat pad. Mice were monitored daily, and tumors were measured twice per week using calipers. All mice were sacrificed on Day 22.

RNA Sequencing Analysis

Single-cell RNA sequencing files containing human newly diagnosed GBM samples and mouse GL261 glioma samples were downloaded from the GEO database with accession number GSE163120.[30] Seurat package (v4.3.0) was used for downstream analysis.[31] In brief, Seurat objects were created from the feature-barcode matrices and annotated by the metadata file provided by the original study. The expression matrices were normalized with a scale factor of 1e6 and scaled. The top 200 variable features were calculated and used for linear dimension reduction by the principal component analysis (PCA). Harmony package (v0.1.1) was used to integrate data from each biological individual.[32] First 20 Harmony dimensions were used to calculate neighbor cells and cell clusters were called by the FindCluster function with a resolution of 0.5. Cell identity of each cluster was determined based on the marker genes provided in the original study. UMAP of cells from human newly diagnosed GBM samples was projected by the DimPlot function. TREM2 expression was plotted by the RidgePlot function. A normalized TREM2 expression matrix was extracted from the Seurat object and examined. The ProjecTILs package was used to determine the identity and ratio ofT cells in the human newly diagnosed GBM samples.[33]

Single-cell RNA sequencing files containing MC38 glioma samples from wild type and *Trem2*$^{-/-}$ mice were also downloaded from GEO database with accession number GSE151710.[3] Seurat objects were created from the feature-barcode matrices and annotated by the metadata file provided by the original study. Tumor-associated macrophages were first subset out according to the annotations described in the original paper and then reannotated with the more detailed macrophage annotation file provided by the original study. The expression matrices were then normalized with a scale factor of 1e6 and scaled. The top 2 000 variable features were calculated and used for PCA. Harmony package (v0.1.1) was used to integrate data from each biological individual. UMAP projection was done using the first 50 dimensions from Harmony. The expression heatmap of selected genes was plotted by the FeaturePlot function in Seurat.

Spectrum Flow Cytometry

Mice were perfused with 40 mL of 1× PBS through intracardiac administration. After perfusion, tumor hemispheres were processed using a previously published protocol for enriching brain infiltrating immune cells, using the Dounce Homogenizer followed by centrifugation on a 30% Percoll (Sigma, P1644-1L) gradient.[34]

Zombie NIR viability dye (1:1 000, BioLegend, 77184) was used to label dead cells. Dissociated cells were further incubated with a with a combination of the following antibodies along with a Fc blocking antibody, rat anti-CD16/CD32 (1:100, BD Pharmingen, 553142): BUV395 anti-F4/80 (1:100, BD Pharmingen, T45-2342), BUV615 anti-NK1.1 (1:100, BD Pharmingen, 751111), BUV805 anti-ICOS (1:100, BD Pharmingen, 568039), BV421 anti-CD62L (1:100, BioLegend, 115537), BV510 anti-CD4 (1:50, BioLegend, 100449), BUV570 anti-CD44 (1:100, BioLegend, 103037), BV605 anti-CTLA4 (1:100 intracellular staining, BioLegend, 106323), BV650 anti-Ly6C (1:100, BioLegend, 128049), BV750 anti-MHCII (1:500, BioLegend, 747458), BV785 anti-CD8α (1:200, BioLegend, 100750), FITC anti-PD-1 (1:100, BioLegend, 135213), Spark Blue 550 anti-Ly6G (1:500, BioLegend, 127663), PerCP anti-CD45 (1:100, BioLegend, 103130), PE-Cy5 anti-CD11b (1:1000, Tonbo, 55-0112-U100),

PE-Fire 700 anti-CD3 (1:200, BioLegend, 100272), APC anti-Foxp3 (1:50 intracellular staining, eBioscience, 17-5773-82), Spark NIR 685 anti-CD69 (1:100, BioLegend, 103277).

Samples were assessed by a spectral flow cytometer (Cytek Aurora, Cytek Biosciences) equipped with SpectroFlo software (Cytek Biosciences). Acquired flow cytometry results were analyzed by FlowJo software (BD Life Sciences).

In vivo 2-photon Imaging

Craniotomy was performed as previously described.[35,36] In brief, under isoflurane anesthesia (3% induction, 1.5%–2% maintenance), a circular craniotomy (<5 mm diameter) was made over somatosensory cortex with the center at about –2.5 posterior and +2 lateral to bregma. A total of 1–2 × 10^3 GL261-luc-mCherry cells in 0.3 µL were injected into the cortex. A circular glass coverslip (4 mm diameter, Warner) was secured over the craniotomy using dental cement (Tetric EvoFlow). A 4-point headbar (NeuroTar) was secured over the window using dental cement. A total of 7–14 days after surgery, we can observe mCherry tumor in the center of the window.

Generation and Culture of Bone Marrow-derived Macrophages

L-929 fibroblasts (Sigma-Aldrich, 85011425-1VL) were cultured in GlutaMaxTM DMEM (Gibco, 10569010), supplemented with 10% FBS, and 1% Penicillin–Streptomycin, to serve as a source of macrophage colony-stimulating factors (M-CSF). Once a sufficient quantity of L-929 culture supernatant was obtained, bone marrow was harvested from WT and *Trem2*$^{-/-}$ mice's femurs and tibias. The extracted bone marrow was cultured in GlutaMaxTM DMEM containing 15% L-929 fibroblast cell culture supernatant which supplied the necessary M-CSF, 10% FBS and 1% Penicillin–Streptomycin. The freshly obtained bone marrow cells underwent a 7-day differentiation period to develop into Bone Marrow-derived Macrophages (BMDMs), with the culture medium refreshed every 72 h.

Phagocytosis Assay

Apoptotic GL261 cells were used to feed the BMDMs. A 2 µM of staurosporine (Abcam, ab146588) was added into the cell culture medium to induce the apoptosis of the GL261 cells 48 h prior to the experiment. The 5 × 10^4 WT and *Trem2*$^{-/-}$ BMDMs were seeded in every well of the 24-well plate 24 h prior to the experiment.

The pHrodo cell labeling kit (Sartorius, 4649) was employed to tag apoptotic GL261 cells with a pH-sensitive fluorophore. Apoptotic GL261 cells were harvested and cleansed using IncuCyte pHrodo Wash Buffer. Following resuspension of the GL261 cells in IncuCyte pHrodo Labeling Buffer, 125 ng/ml of pHrodo red cell labeling dye was introduced, and incubation was carried out at 37°C for 1 h. After dual washing steps, 5 × 10^4 GL261 cells were added to each well of a 24-well plate and co-cultured with BMDMs for 0, 2, 3, and 4 h.

Following internalization by phagocytes, pHrodo red-labeled cells, situated in the neutral extracellular milieu (pH 7.4), undergo a transformation within the acidic phagosome (pH 4.5–5.5), resulting in a noticeable enhancement of red fluorescence emission. Subsequently, BMDMs were collected for flow cytometry analysis to quantify phagocytosis by evaluating the mean fluorescence intensity (MFI) of the red fluorescence.

In vitro Antigen Presentation Assay

BMDMs were reseeded into 24-well plates at a density of 3 × 10^5 cells per well. The cells were then exposed to 10 µg/mL ovalbumin (sigma A5503) for a duration of 6 h, followed by treatment with 100 ng/ml LPS for 18 h. Subsequently, the BMDMs were washed with fresh medium and co-cultured for 3 days with purified carboxyfluorescein diacetate succinimidyl ester (CFSE)-labeled naïve OT I CD8 T cells or naïve OT II CD4 T cells at a 1:1 ratio. Following a 5-day incubation period, T cells were subjected to flow cytometry analysis to assess CFSE dilution in viable $CD3^+CD4^+$ or $CD8^+$ lymphocytes.

In vivo $CD4^+$ T-Cell Depletion

Mice were subjected to intraperitoneal (IP) injections of a 200 µg anti-CD4 depleting antibody (clone GK1.5, catalog #BE0003-1, BioXcell). The initial injections were administered on both Day 10 and Day 11 after brain tumor inoculation. Subsequently, injections were administered at 5-day intervals to sustain the depletion of $CD4^+$T cells throughout the entire study period. The control group received IgG (I4131-10MG) at the same dosage.

Formalin-fixed Paraffin-embedded (FFPE), Cryosection, Immunofluorescence Staining and Confocal Imaging

FFPE was used to embed endpoint tumor brains, to reduce autofluorescence of CD4 staining in tumor core regions. After 24–48 h of fixation, tissues were dissected, and placed in embedding cassettes. Fixed tissues were then transferred to 70% ethanol and processed as follows: 70% ethanol for 1 h, 85% ethanol for 1 h, 95% ethanol for 3 × 30 min, 100% ethanol for 3 × 30 min, and xylene 3 × 30 min. After xylene, tissues were embedded into paraffin at 60°C across 4 changes, 2 × 45 min, 2 × 60 min. Tissues were immersed in liquid throughout the process.

Brain sections (5 µm) were obtained by a Leica microtome. Paraffin was removed from samples by consecutive 2 × 10 min washes with xylene. Xylene was then removed with graded washes of ethanol to water (100% ethanol 3 × 3 min, 96% ethanol 2 × 3 min, 85% ethanol 1 × 3 min, 70% ethanol 1 × 3 min, and ddH_2O 20s). The samples were immediately subjected to antigen retrieval using Tris EDTA buffer (pH = 9) at 70°C for 60 min. After cooling down, we removed the antigen retrieval buffer and washed the slides with PBS.

To evaluate mCherry tumor signals during the early stages of tumor development, PFA-perfused tumor

hemispheres underwent a 30% sucrose dehydration process followed by cryosection.

For immunostaining, the slides were blocked by 4% of bovine serum albumin (EMD Millipore Corp, 126615-25 mL) in PBS with 0.2% Tween-20. Primary antibodies were stained overnight in 4°C with rat anti-CD4 (1:100, Invitrogen, 14-9766-82) and rabbit-anti-Iba1 (1:500, Abcam, Ab178847). Slides were incubated with secondary antibodies of goat-anti-rat 488 and goat-anti-rabbit 594 (1:500, Invitrogen, A11006, A11037) for 1.5 h at room temperature. Sections were washed and mounted with DAPI Fluoromount-G mounting medium (SouthernBiotech). Fluorescent images were obtained by a confocal microscope (LSM 980, Zeiss). Cell counting was manually quantified, and brightness and contrast were adjusted by ImageJ (National Institutes of Health). A 3D reconstruction was generated using IMARIS.

RNA Extraction and Quantitative Reverse Transcription Polymerase Chain Reaction (qRT-PCR)

RNA was extracted from the endpoint hemispheres using RNAeasy Plus Mini Kit (Qiagen, 74134). Reverse transcription of RNA was performed using iScript cDNA Synthesis Kit (Bio-Rad, 1708891). cDNA was added to a reaction mix (20 µL final volume) containing gene-specific primers and SYBR Green Supermix (Bio-Rad, 1725271). All samples were run in duplicates in LightCycler 480 II (Roche). The relative gene expression was normalized to *Gapdh* and assessed using the $2^{-\Delta\Delta CT}$ method. Primer sequences and information are as follows (5′–3′): *Gapdh*: CATCTTCCAGGAGCGAGACC (forward), TCTCGTGGTTCACACCCATC (reverse); *Trem2*: CTCCAGGAATCAAGAGACCTCC (forward), CCGGGTCCAG TGAGGATCT (reverse); *Cd68*: TGTCTGATCTTGCTAGGA CCG (forward), GAGAGTAACGGCCTTTTTGTGA (reverse); *H2-Aa*: TCAGTCGCAGACGGTGTTTAT (forward), GGGGG CTGGAATCTCAGGT (reverse); *Cd4*: AGGTGATGGGACCTA CCTCTC (forward), GGGGCCACCACTTGAACTAC (reverse).

Statistical Analysis

GraphPad Prism 9 was used for statistical analysis. All results were reported as mean with standard error of the mean (SEM). The data were tested for normal distribution using Shapiro–Wilk test first. *P*-values were acquired using 2-tailed Student *t* tests or 2-way ANOVA if the data were normally distributed, or Mann–Whitney test if they were not. Survival curves were analyzed using log-rank test. Mice were of mixed sexes. Mice within experiments were age and sex-matched.

Results

Brain Tumors Exhibit Significantly Higher Levels of *TREM2* Expression, Predominantly in Tumor-associated Myeloid Cells

To understand the potential relevance of TREM2 in cancer, first, we explored the *TREM2* expression profile across multiple tumor samples through the GEPIA portal.[37] Interestingly, we found a prevalent increase of *TREM2* in 22 tumor types compared to the paired normal tissues (Supplementary Table 1). Brain tumors exhibited remarkably elevated levels of *TREM2* expression compared to other tumor types (GBM: median = 117.85 transcripts per million (TPM); LGG: median = 54.32 TPM; Figure 1A). Although recent studies have demonstrated that *TREM2* is linked to worse outcomes in peripheral murine tumors, including sarcoma, colon adenocarcinoma, and breast adenocarcinoma,[3,21,22] research on TREM2 in brain tumors remains limited. To investigate the potential role of TREM2 in glioma, we first queried *TREM2* expression patterns at the cellular level using a recently published glioma data set.[30] When a tumor occurs, there is a massive infiltration of immune cells into the tumor mass. We examined a total of 21,303 $CD45^+$ immune cells from human newly diagnosed GBM and categorized them into 9 distinct immune populations based on their marker genes (Supplementary Figure 1A). The majority of immune populations are tumor-associated myeloid cells, comprising approximately 80% of the immune cells (Figure 1B). These tumor-myeloid cells were composed of 2 main populations, microglia and macrophages. Among all immune cell populations, *TREM2* was expressed in almost all microglia, with the highest levels of transcription observed in these cells (Figure 1C and D). *TREM2* expression was also detected in multiple subtypes of macrophages and some extent in other immune cells including lymphocytes. Although TREM2 is mostly expressed in immune cells, we still need to confirm whether tumor cells could be the source of TREM2. Our analysis based on clinical sample data set[38] showed that CD45 negative cells from dissected human *IDH*WT gliomas, which are likely to be actual tumor cells, have no TREM2 expression compared to tumor-associated microglia and macrophages as positive controls of TREM2 expression (Figure 1E).

We extended our investigation to the TCGA data set, which provides a larger cohort of patients, to analyze the correlation between TREM2 expression and tumor-myeloid features as well as functional genes. Our analysis of human gliomas (LGG and GBM) revealed a strong correlation between *TREM2* expression levels and tumor-associated myeloid markers, such as *AIF1* (encoding IBA1), *ITGAM* (encoding CD11B), and *CD14* (Figure 1F). This suggested that higher levels of *TREM2* expression were associated with increased myeloid infiltration. Additionally, although TREM2 was linked to tumor immunosuppression in recent studies,[39] we found that immunosuppressive markers including *ARG1* (encodes Arginase 1), and *CD274* (encodes programmed death-ligand 1 (PD-L1), an immune inhibitory receptor ligand) were poorly associated with *TREM2* expression (Figure 1F). In line with known TREM2 function in phagocytosis in the neurodegeneration field, we found that *CD68* (encodes a heavily glycosylated glycoprotein predominantly expressed in late endosomes and lysosomes of macrophages) was strongly correlated with *TREM2* expression. Furthermore, genes involved in antigen-presenting pathways such as *ITGAX* (encodes integrin alpha X chain protein CD11C, a marker of antigen-presenting cells), *CD86* (provides costimulatory signals necessary for T-cell activation and survival), *CIITA* (MHC Class II transactivator, responsible for turning on MHC

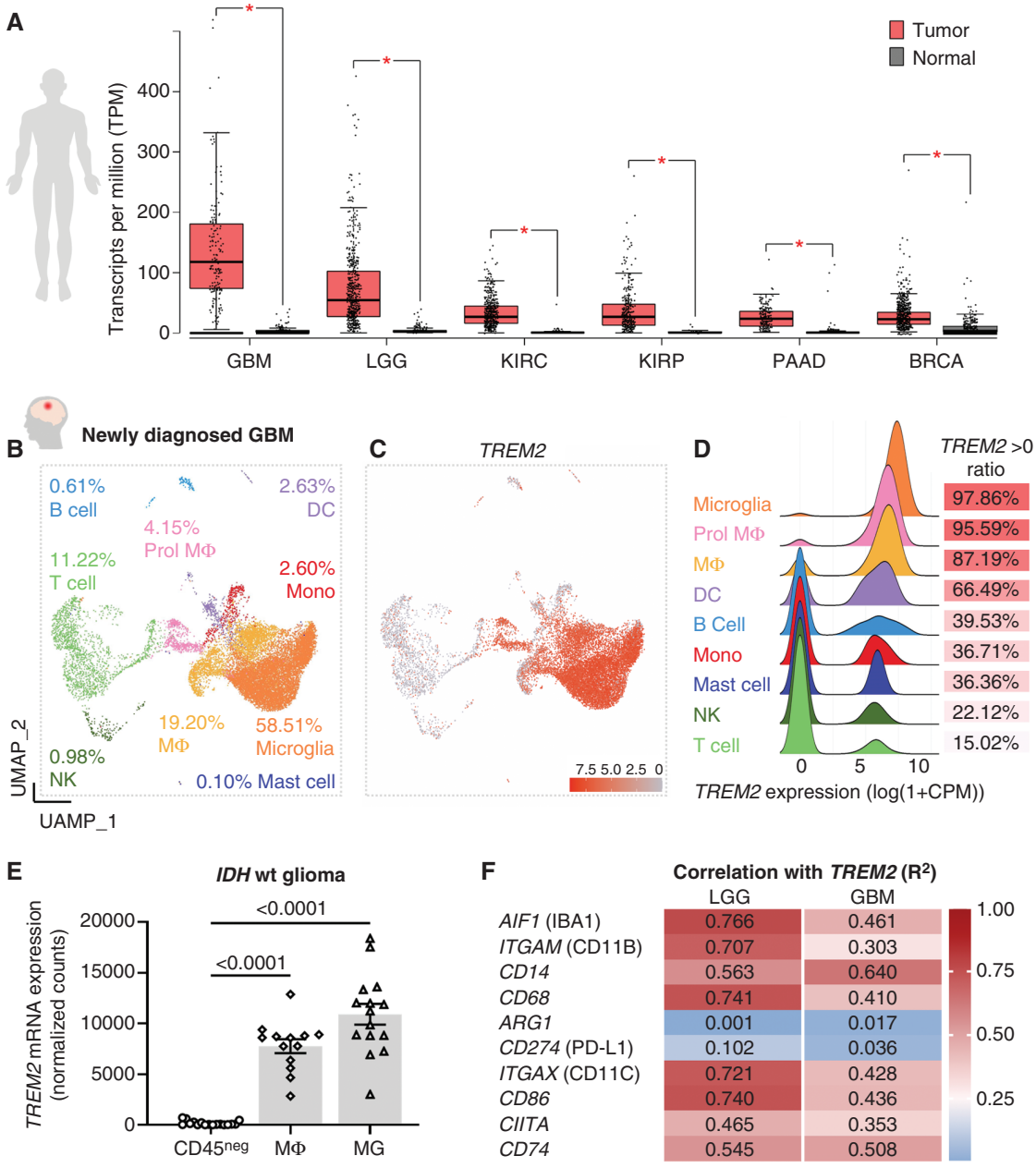

Figure 1. Brain tumors exhibit significantly higher levels of TREM2 expression, predominantly in tumor-associated myeloid cells. (**A**) Top 6 types of tumors with elevated *TREM2* expression in a descending order from left to right, which were glioblastoma (GBM), brain lower grade glioma (LGG), kidney renal clear cell carcinoma (KIRC), kidney renal papillary cell carcinoma (KIRP), pancreatic adenocarcinoma (PAAD), and breast cancer (BRCA). (**B**) UMAP plots displaying the immune cells in patients with newly diagnosed GBM. (**C, D**) *TREM2* transcription in different immune cell populations. (**E**) *TREM2* is not detected in brain tumor cells. The data were shown as mean ± SEM and analyzed by 1-way ANOVA. (**F**) The correlation between *TREM2* expression and signature genes related to myeloid cell phagocytosis, immunosuppression, and antigen presentation was evaluated in LGG and GBM patients. The Spearman's correlation test produces both *P*-values and correlation coefficients (R^2). All listed genes had a *P*-value of less than 0.05. Genes with an R^2 value greater than 0.25 were considered to have a correlation (either positive or negative) with *TREM2* expression.

Class II gene transcription), and *CD74* (the invariant chain required for the proper folding and trafficking of MHC Class II in antigen-presenting cells), were well-correlated with *TREM2* expression (Figure 1F). These findings underscore the potential involvement of TREM2 in phagocytosis and antigen presentation in glioma.

TREM2 Deficiency Does Not Slow Brain Tumor Progression

To investigate whether TREM2 contributes to glioma progression, we used an immunocompetent glioma model by inoculating 5×10^4 GL261 cells into the brains of both

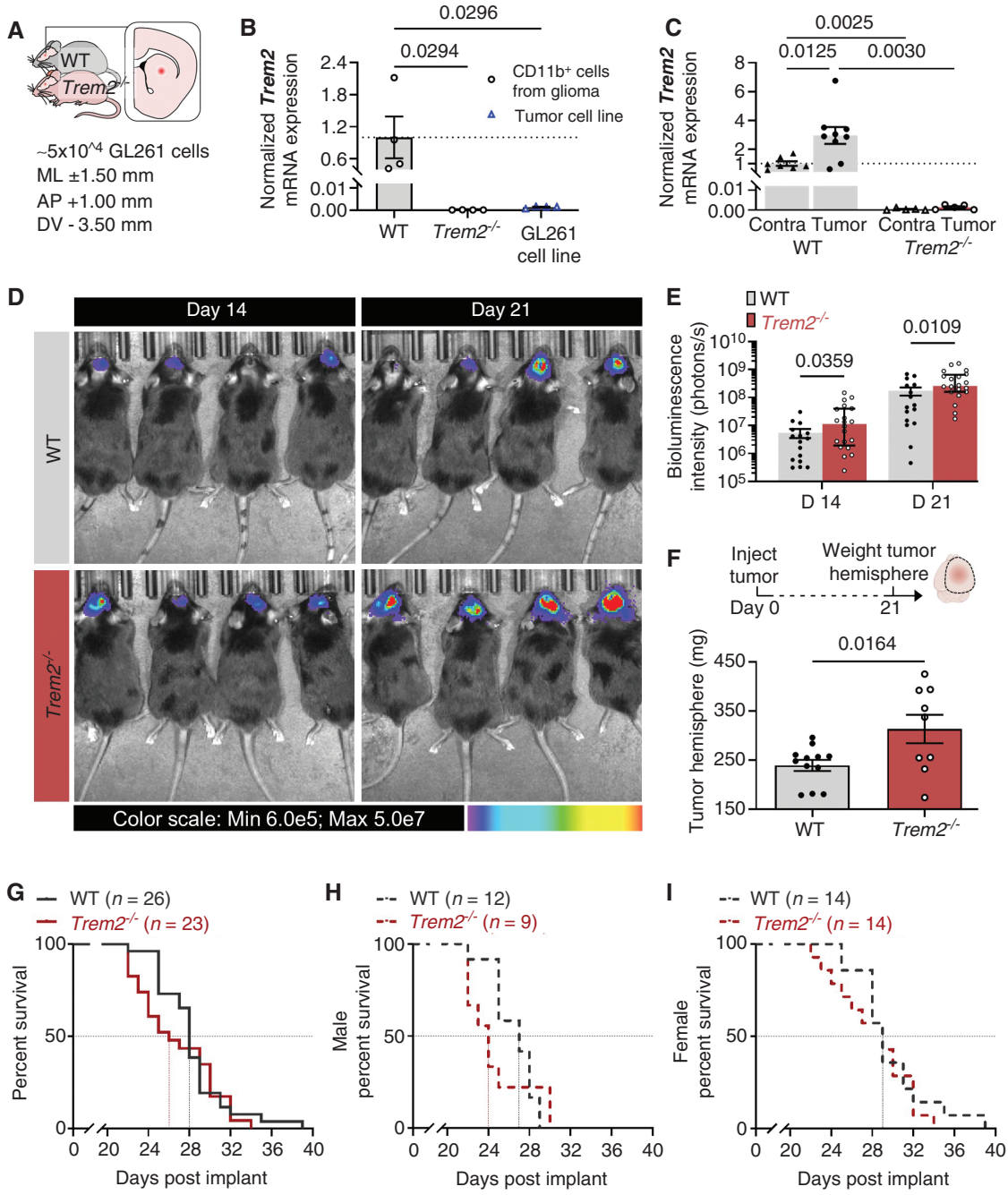

Figure 2. TREM2 deficiency does not slow mouse glioma progression. (**A**) A schematic illustration of establishing an immunocompetent glioma model using murine glioma GL261 cells. (**B**) To determine the expression of *Trem2* in the GL261 cell line, CD11b$^+$ cells were sorted from gliomas of both WT and *Trem2*$^{-/-}$ mice, serving as positive and negative controls, respectively. (**C**) The mRNA levels of *Trem2* in the contralateral and tumor hemispheres were quantified by qRT-PCR. (**D, E**) Bioluminescence imaging was used to track and monitor the same mice over a period of 21 days. The statistical analysis showed that brain tumor burden was relatively higher in *Trem2*$^{-/-}$ mice compared to WT mice. (**F**) A larger tumor size was observed in *Trem2*$^{-/-}$ mice compared to the WT mice 21 days after tumor inoculation, as indicated by the increased weight of tumor hemisphere. (**G–I**). The survival study using 26 WT (12 males and 14 females) and 23 *Trem2*$^{-/-}$ (9 males and 14 females) mice showed Trem2 deficiency did not confer any survival benefit in glioma. The data were shown as mean ± SEM. The data were tested for normal distribution using Shapiro–Wilk test first. *P*-values were acquired using 2-tailed Student *t* tests or 2-way ANOVA if the data were normally distributed, or Mann–Whitney test if they were not. Survival curves were analyzed using log-rank test.

WT and *Trem2*$^{-/-}$ mice (Figure 2A). We first confirmed that TREM2 is absent in mouse glioma cells both *in vitro* (Figure 2B) and *in vivo* (Figure 2C). Additionally, there is a significant increase in *Trem2* expression in WT tumor hemispheres compared to contralateral hemispheres (Figure 2C). Next, we measured the glioma growth by

bioluminescence imaging and the weight of the tumor hemispheres (Figure 2D–F). Using bioluminescence imaging to monitor the same mice, our result revealed a slightly higher burden of brain tumors in *Trem2*$^{-/-}$ mice compared to WT animals at both Day 14 and Day 21 post-tumor inoculation (Figure 2D and E). Consistent with the bioluminescence result, a larger tumor size was observed in *Trem2*$^{-/-}$ mice compared to the WT mice, as evidenced by the increased weight of the tumor hemisphere at Day 21 post-tumor inoculation (Figure 2F). A survival study using 26 age-matched WT (14 females and 12 males) and 23 *Trem2*$^{-/-}$ mice (14 females and 9 males) showed that *Trem2* deficiency did not improve glioma survival, and even resulted in a slightly shorter median survival time compared to the WT (Figure 2G). We acknowledge that the slightly increased tumor burden in *Trem2*$^{-/-}$ mice does not significantly affect the survival curves, as survival curves are typically measured by the 50% death rate and do not account for the full range of survival times.This conclusion was consistent regardless of whether the data was analyzed by sex (Figure 2H and I). In addition to the GL261 model, we conducted an experiment utilizing the 73C astrocyte-derived glioma model (Supplementary Figure 2A). Similar to that in the GL261 model, the tumor burden of the 73C glioma was found to be elevated in *Trem2*$^{-/-}$ mice (Supplementary Figure 2B). Furthermore, an independent research team employed the CT2A brain tumor model and arrived at analogous conclusions.[40] Thus, a comprehensive analysis of 3 distinct brain glioma models collectively demonstrates that TREM2 deficiency does not impede intracranial tumor progression.

The observed phenotype within the preclinical glioma models contrasts with findings from various peripheral tumor models, where *Trem2*$^{-/-}$ mice exhibited a decelerated rate of tumor progression.[3,21,22] To discern whether the discrepancy was potentially due to the tumor locations, we repeated the same experiments using the MC38 subcutaneous model with 9 WT and 8 *Trem2*$^{-/-}$ mice (Supplementary Figure 2C). In line with previous findings,[3] we observed a clear trend toward attenuated tumor progression in *Trem2*$^{-/-}$ mice (Supplementary Figure 2D). Individual plots (Supplementary Figure 2E and F) showed that despite variations within the *Trem2*$^{-/-}$ group, these mice displayed an attenuated trend in tumor progression compared to the WT, with some even exhibiting tumor regression. Taken together, our findings suggest that the role of TREM2 in brain tumors may differ from that in peripheral tumors. Although TREM2 in peripheral tumors is detrimental, it may have unrecognized protective roles specific to brain tumors, highlighting the need for further investigation.

TREM2 Deficiency Reduces the Ability of Tumor-associated Myeloid Cells to Phagocytose Tumors

We next examined 27,276 WT immune cells[30] from mouse GL261 glioma at Day 21 post inoculation to map *TREM2* transcription in immune cells. Similar to newly diagnosed human GBM, tumor-associated myeloid cells constituted the largest immune cell population in GL261 glioma, accounting for approximately 65% of the total immune cells (Figure 3A and Supplementary Figure 1B). Additionally, the proportion of macrophages was much higher (49.98%) compared to microglia (7.85%). Among all immune cell populations, *TREM2* was highly expressed in almost all microglia, and multiple subtypes of macrophages (Figure 3B and C).

The observed correlation between *TREM2* expression and phagocytic and antigen-presenting markers in human gliomas prompted an *in vivo* exploration to assess the extent of TREM2's impact on promoting a glioma-mediated immune response. To determine whether TREM2 deficiency impairs myeloid cell phagocytosis in brain tumors, we took advantage of *in vivo* 2-photon imaging. After transducing the GL261 tumor cell line with mCherry labeling, we injected them into the somatosensory cortex of *Cx3cr1*$^{Gfp/+}$ mice after craniotomy. Between 7 and 14 days after tumor inoculation, we observed CX3CR1^{GFP} myeloid cells closely interacting with tumor cells in the tumor core region. Interestingly, some of these myeloid cells were observed to uptake mCherry^{+} tumor debris and persisted for hours (Figure 3D). To assess potential variations in mCherry debris signal in the absence of TREM2, brain samples were collected 12–14 days after tumor inoculation for immunostaining (Supplementary Figure 3A). Notably, tumor-associated myeloid cells, marked by pan-myeloid marker IBA1, exhibited diverse patterns of mCherry signal distribution within their cytosol. Specifically, observations revealed a spectrum of occurrences: instances devoid of detectable mCherry signals (Figure 3E, Cells 1 and 4; Supplementary Figure 3B, Cell 4), instances characterized by the presence of discrete mCherry^{+} puncta within the cytosol (Figure 3E, Cell 3; Supplementary Figure 3B, Cells 1, 2, and 3), and instances exhibiting a spherical morphology alongside condensed DAPI staining (Figure 3E, Cells 2 and 5). These intracellular mCherry signals were evident in structures resembling tumor debris or aligned with the characteristics of apoptotic cells.[41] Furthermore, through an analysis of myeloid cell dimensions and mCherry content, we discerned that the occurrence of mCherry signals varies across different sizes of myeloid cells. In addition, the presence of red signals was diminished in myeloid cells lacking TREM2 (Figure 3F and Supplementary Figure 3B). These mCherry signals can also be detected by flow cytometry (Supplementary Figure 3C). Consistent with the immunostaining result, we found the mCherry signals were colocalized with MHCII^{+}F4/80^{+} antigen presenting like macrophages, with a higher MFI in WT compared to *Trem2*$^{-/-}$ mice (Figure 3G and G′ and Supplementary Figure 3D).

As *in vivo* phagocytosis could be influenced by tumor size, we also established a more controlled environment by employing BMDM to investigate the potential impact of TREM2 on tumor phagocytosis. In this experimental setup, GL261 tumor cells were subjected to a 2 μM staurosporine treatment to induce apoptosis. After a 48-h interval, the resulting apoptotic tumor cells were harvested, labeled with pHrodo red dye, and subsequently introduced to WT and *Trem2*$^{-/-}$ BMDM for phagocytic analysis (Supplementary Figure 3E). In the sequence of phagocytosis events, the pHrodo dyes underwent a shift from a nearly nonfluorescent state under neutral pH conditions to manifesting a progressively intense red fluorescence

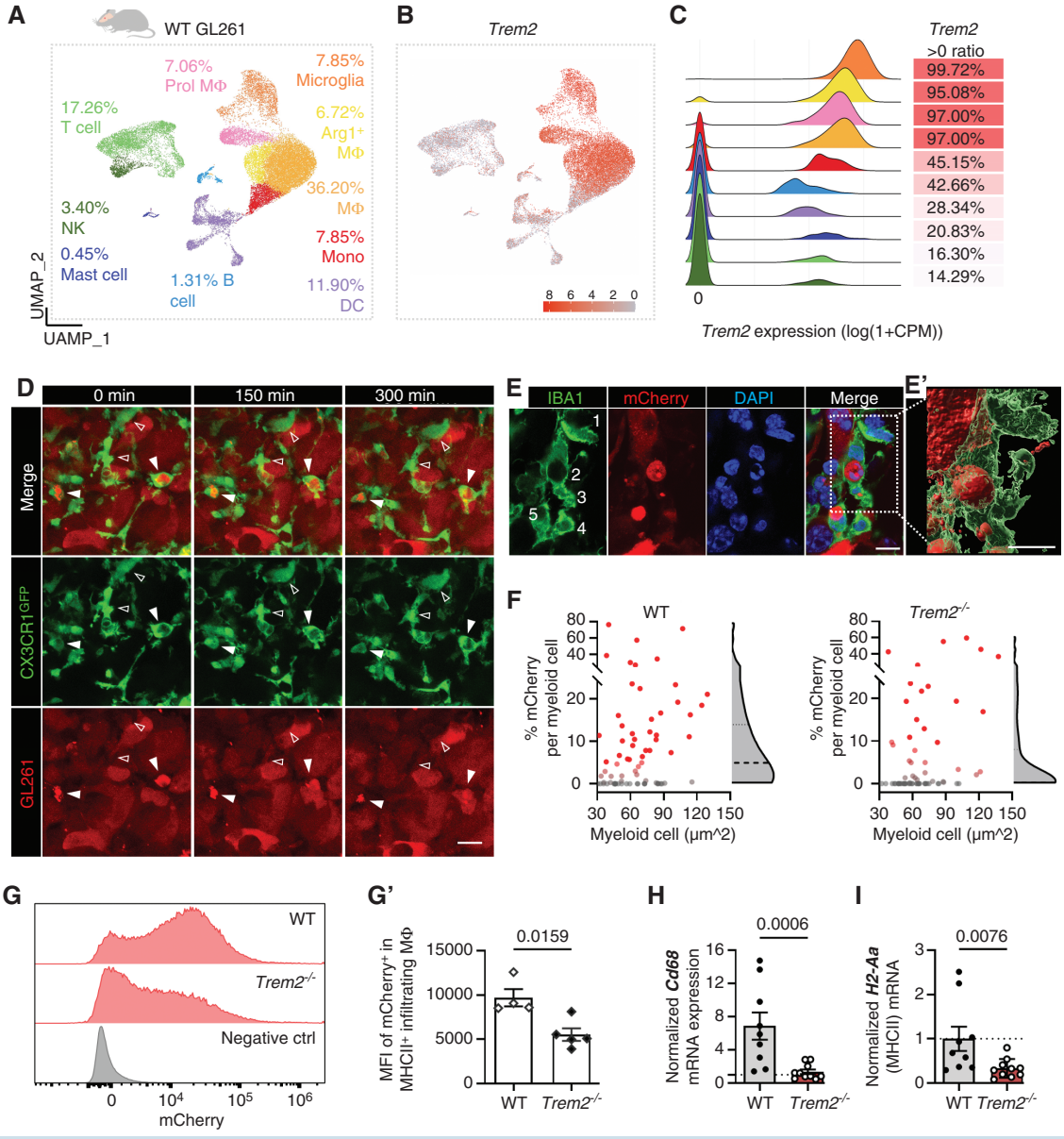

Figure 3. TREM2 deficiency reduces the ability of tumor-associated myeloid cells to phagocytose tumors and exhibit MHC Class II expression. (**A**) UMAP plots displaying the immune cells in mice with glioma GL261. (**B, C**) *TREM2* transcription in different immune cell populations. (**D**) Through *in vivo* 2-photon imaging, interactions between CX3CR1^{GFP} myeloid cells and mCherry^{+} tumor cells were observed. Solid triangles indicate myeloid cells that uptake red tumor debris and hollow triangles indicating those that do not. Scale bar: 10 μm. (**E**) Immunostaining revealed a diverse mCherry signal distribution within the cytosol of tumor-associated myeloid cells, identified by the pan-myeloid marker IBA1. These observations delineated a spectrum of patterns: Cells 1 and 4 lacked discernible mCherry signals, Cell 3 showcased discrete mCherry^{+} puncta within the cytosol, and Cells 2 and 5 displayed a spherical morphology accompanied by condensed DAPI staining. (**E'**) IMARIS-generated 3D reconstruction demonstrates distinct patterns of mCherry signal in Cell 1, 2, and 3. (**F**) An analysis of myeloid cell dimensions and mCherry content revealed variations in the occurrence of mCherry signals across different sizes of myeloid cells. Each tumor mouse contributed 15 cells, and each group consisted of 5 mice. The distribution is depicted in the violin plot, highlighting that the absence of TREM2 in myeloid cells led to a reduction in the presence of mCherry signals. (**G, G'**) Measurement of the MFI of mCherry^{+} tumor debris signal in F4/80^{+}MHCII^{+} macrophages. The percentage of tumor debris signal in F4/80^{+}MHCII^{+} macrophages was reduced in *Trem2*$^{-/-}$. (**H, I**) The mRNA levels of *Cd68* and *H2Aa* (encoding MHC Class II) in the endpoint tumor hemispheres were collected and quantified by qRT-PCR. The bar graphs were shown as mean ± SEM. The data were tested for normal distribution using Shapiro–Wilk test first. *P*-values were acquired using 2-tailed Student *t* tests if the data were normally distributed, or Mann–Whitney test if they were not.

within the acidic phagosome environment. BMDMs subjected to the treatment were collected at timepoints of 0, 2, 3, and 4 h for flow cytometry analysis. We observed a progressive rise in the mean fluorescent intensity (MFI) of red fluorescence over time. Notably, at the 4-h timepoint, the MFI of WT was higher than *Trem2*$^{-/-}$ (Supplementary

Figure 3G and H). Collectively, our results showed that TREM2 deficiency reduces the capacity of tumor-associated myeloid cells to engage in phagocytose (Supplementary Table 1 and Figures 1–6) tumors.

TREM2 Deficiency Reduces Tumor-associated Myeloid Cell MHC Class II Expression

Because MHC Class II presentation is generally derived from exogenous proteins, we further investigated whether TREM2 affects the tumor-myeloid MHC Class II expression. We extracted RNA from tumor hemispheres at the humane endpoint of the mouse survival study when the glioma reached its maximum size. We found that *Cd68* expression in the WT tumor hemispheres was significantly higher than in the *Trem2*$^{-/-}$ tumor hemispheres (Figure 3H). The *H2-Aa*, which encodes mouse Class II antigen A, was also significantly lower in the *Trem2*$^{-/-}$ tumor hemispheres than the WT ones (Figure 3I).

To better understand how TREM2 deficiency affects myeloid cell responses concerning MHC Class II, we initiated our analysis by examining WT and *Trem2*$^{-/-}$ tumor-associated myeloid cells, utilizing a dataset derived from Day 10 MCA/1956 tumors.[3] Myeloid cells were clustered into 8 subsets using Uniform Manifold Approximation and Projection (UMAP; Supplementary Figure 4A). Cluster 5 (CX3CR1-Macs) and Cluster 6 (Cycling-Macs), which were poorly represented in *Trem2*$^{-/-}$ mice, exhibited particularly high *Trem2* expression. These 2 clusters showed a more macrophage-like profile with high levels of *Cx3cr1* and *Mrc1*, but low levels of *Ly6c2* and *Ccr2*. They also expressed lysosome markers *Cd68*, and antigen-presenting cell markers *Cd86* and *H2-Ab1* (Supplementary Figure 4B). These findings suggested that TREM2 deficiency induces alterations within myeloid cell subsets in response to tumors. Notably, this deficiency may lead to a decrease in a specific subset of myeloid cells characterized by both high TREM2 expression and antigen-presenting features.

To further validate what we observed from the single-cell sequencing data, we performed flow cytometry on Day 25 when most mice had a high tumor burden. Unbiased UMAP clustering of high parameter flow cytometry data obtained from total immune cells (CD45^{+}) of PBS-perfused tumor hemispheres identified 7 main clusters, including microglia, infiltrating myeloid, CD8^{+} T cells, natural killer cells (NK), B cells, regulatory T (Treg), and conventional T helper (Th) cells (Supplementary Figure 4C). As the tumor size increased, the percentage of microglia in WT mice decreased due to the influx of other immune cells (Supplementary Figure 4D). However, the percentage of microglia was already low in *Trem2*$^{-/-}$ mice and further decreased with increasing tumor size. This observation suggests that *Trem2*$^{-/-}$ microglia may have impaired activation in response to the tumor at the onset, leading to a lower proportion of microglia in the tumor microenvironment. The higher percentage of infiltrating cells in *Trem2*$^{-/-}$ mice may be a compensatory response to the impaired microglia activation. In infiltrating immune cells (CD45^{hi}), infiltrating myeloid, NK cells, and lymphocytes weighted similarly in WT and *Trem2*$^{-/-}$ (Supplementary Figure 5A–D). WT and *Trem2*$^{-/-}$ showed a similar trend of increased percentage of infiltrating myeloid, and a decreased percentage of NK and lymphocytes along with increased tumor size. We further delved into the influence of TREM2 on infiltrating myeloid subsets. Consistent with findings of TREM2 deficient macrophages in MCA/1956 tumors (Supplementary Figure 4B), a Ly6C^{neg}F4/80^{+} cluster with high CD68 and MHC Class II expression was reduced in *Trem2*$^{-/-}$ mice (Supplementary Figure 4E and F). This MHC II^{hi} macrophage-like subset was positively correlated with the tumor size. However, the percentage of this antigen-presenting-like macrophage subset was much higher in WT, particularly in high tumor burden hemispheres (more than 250 mg), compared to that in *Trem2*$^{-/-}$ mice (Supplementary Figure 4G). Collectively, our findings suggested that TREM2 deficiency leads to a reduction in MHC Class II expression within myeloid cells.

TREM2 Deficiency Impairs CD4^{+} T-Cell Responses to Gliomas

Considering CD4^{+} T cells' engagement with antigen-presenting cells, we next determine whether TREM2 deficiency in the mouse model of glioma could affect CD4^{+} T-cell infiltration. To ascertain the significance of CD4^{+} T-cell involvement in regulating tumor size within the GL261 glioma model, we initiated an investigation involving the depletion of CD4^{+} T cells using an anti-CD4^{+} antibody. We administered 200 μg of the anti-CD4 depleting antibody or control-IgG through IP injections on days 10, 11, 16, and 21 (Supplementary Figure 6A). The mice that underwent CD4^{+} cell depletion exhibited a significantly increased tumor burden (Supplementary Figure 6B). This observation aligns with previous studies[42] that underscore the critical role of CD4^{+} cells in regulating tumor growth. Delving further into this aspect, we examined the variance in CD4 expression within the trem2 context and found that *Cd4* expression in WT glioma-endpoint hemispheres was higher compared to that in *Trem2*$^{-/-}$ mice (Figure 4A). This was corroborated by immunofluorescence staining of CD4 at the endpoint hemispheres, which consistently demonstrated a greater number of CD4^{+} T cells in WT mice than in *Trem2*$^{-/-}$ mice (Figure 4B). In addition, we found that CD4^{+} T cells were mostly located in the tumor region and were in contact with macrophages (Iba1^{+}, ramified structure) with varying proximities and interactions (Figure 4C). In WT, approximately 16% of CD4^{+} T cells had no cell-to-cell contact with macrophages, 17% had some interaction via the tips of macrophage processes, 58% had tight interaction between cell soma, and 8% were enclosed by multiple macrophages. In *Trem2*$^{-/-}$ mice, CD4^{+} T cells had decreased intermediate contact with macrophages and increased enclosed-type interaction (Figure 4C and D). The formation of intermediate/tight contacts between T cells and antigen-presenting cells is thought to be a result of antigen stimulation,[43] whereas the enclosed structure is likely to represent macrophage uptake of exhausted T cells. Thus, these results suggest that TREM2 in the antigen-presenting-like macrophage subset is critical for the interaction with CD4^{+} T cells in gliomas.

Upon analyzing infiltrating T-cell composition using flow cytometry, we surprisingly found that the higher number of CD4^{+} T cells in WT mice was primarily due to Treg

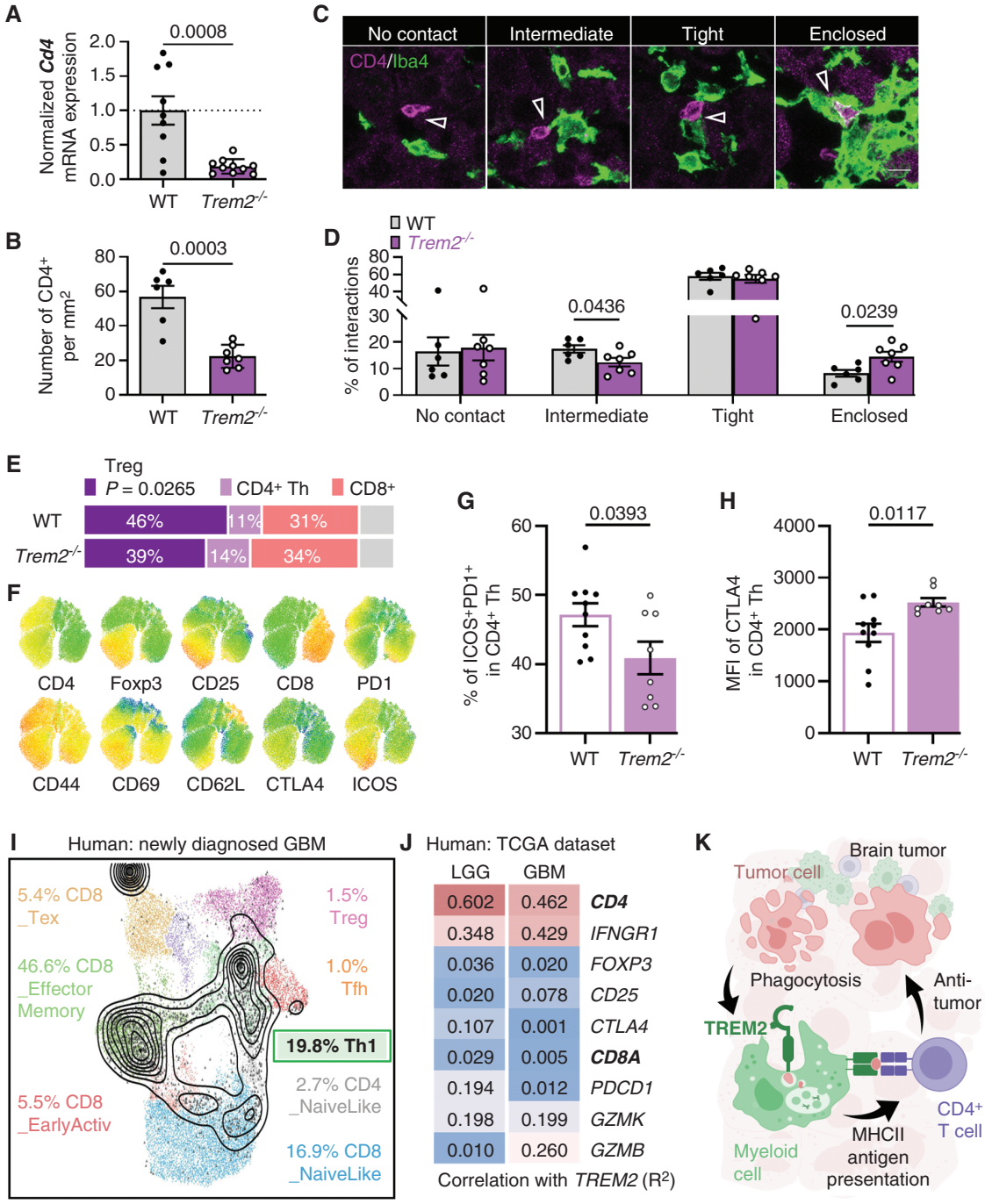

Figure 4. TREM2 is necessary for accumulation of CD4⁺ T cells in brain tumors. (**A**) Quantification of *CD4* mRNA levels in tumor hemispheres using qRT-PCR. (**B**) Quantification of the number of CD4⁺ T cells per mm² in the tumor core using confocal microscopy on 5 µm thick brain slides. (**C**) Representative images of CD4⁺ T cell and myeloid cell (Iba1⁺) interactions. Scale bar: 10 µm. (**D**). Quantifications of different types of CD4⁺-myeloid cell interactions in WT and *Trem2*$^{-/-}$. (**E**). The percentage of each CD3⁺ T cell subset in WT and *Trem2*$^{-/-}$ mice. Unidentified populations are indicated in gray. (**F**) Expression levels of T cell cluster markers and feature genes indicating T cell activation or immunosuppression. (**G**). The proportion of a CD4⁺ Th cell subset co-expressing PD-1 and ICOS is greater in WT mice compared to *Trem2*$^{-/-}$ mice. (**H**) The MFI of CTLA expression in CD4⁺ Th cells was higher in *Trem2*$^{-/-}$ compared to the WT. The bar graphs were shown as mean ± SEM. The data were tested for normal distribution using Shapiro–Wilk test first. *P*-values were acquired using 2-tailed Student *t* tests if the data were normally distributed, or Mann–Whitney test if they were not. (**I**) Projection of T cells from newly diagnosed GBM using the ProjecTIL package to reveal T-cell subsets. (**J**) Correlation between *TREM2* expression and marker genes of T cell subtypes in LGG and GBM patients. All listed genes, except for *CTLA4*, had a *P*-value less than 0.05. (**K**) Our working model proposes that TREM2-mediated phagocytosis of glioma debris by myeloid cells leads to further MHC Class II presentation to CD4⁺ T cells, ultimately contributing to antitumor immunity in brain tumors.

(CD25+Foxp3+; Figure 4E). However, no notable distinction was observed in the proportion of CD8+ T cells between WT and *Trem2*$^{-/-}$. We further investigated various T-cell markers and found that the Treg cluster expressed a mixture of markers that positively regulated T-cell activation[44,45] such as CD44+, ICOS+, CD69+, CD62L+, as well as negative regulatory markers such as CTLA4+ (Figure 4F). Therefore, this population could potentially have both anti- and protumoral functions.

Despite the unchanged percentage of CD4+ Th cells, we observed a higher presence of a CD4+ Th cell subset co-expressing PD-1 and ICOS in WT compared to *Trem2*$^{-/-}$ (Figure 4G). This subset was demonstrated to recognize both tumor-associated antigens and tumor-specific neoantigens, contributing to antitumor responses.[45] On the other hand, we found that the expression level of CTLA in CD4+ Th cells was higher in *Trem2*$^{-/-}$ compared to the WT (Figure 4H). This observation suggested a potential downregulation of CD4+ Th antitumor responses in *Trem2*$^{-/-}$. To gain further insights into TREM2's function in antigen presentation, we conducted co-culture experiments involving naïve OT I CD8+ T cells and naïve OT II CD4+ T cells with OVA-fed BMDMs from WT or *Trem2*$^{-/-}$. By subjecting the BMDMs to this model antigen, they processed and presented antigen fragments to OT I CD8+ T cells via MHC I or to OT II CD4+ T cells via MHC II. Consequently, T cells recognizing antigens were activated, as evidenced by their proliferation. We observed that when co-cultured with OVA-fed Trem2-deficient BMDMs, only OT II CD4+ T cells exhibited decreased proliferation, but not OT I CD8+ T cells (Supplementary Figure 6C and D).

To further address the significance of CD4+ T cells in human gliomas, we analyzed T-cell composition in newly diagnosed GBM. We projected all the GBM T cells[30] onto a T cell reference atlas provided by the ProjecTIL package[33] to reveal T-cell subsets. We found that Th1-like CD4+ T cells were the second largest population in the newly diagnosed GBM T cells after effector memory CD8+ T cells, accounting for 19.8% of the total GBM T cells (Figure 4I). Furthermore, analysis of the TCGA data set revealed a correlation between *TREM2* and Th1-like markers such as *CD4* and IFN-gamma receptor 1 (*Ifngr1*) in both LGG and GBM (Figure 4J). However, no significant correlation was found between TREM2 expression and Treg markers such as *FOXP3* and *CD25* (also known as *IL2RA*), or immunosuppressive markers such as *CTLA4*. Additionally, markers of effector memory CD8+ T cells such as *PDCD1* and granzymes (mostly *GZMK*, with an intermediate level of *GZMB*) showed minimal correlation with TREM2 expression. Collectively, these results suggest a positive role of TREM2 in mediating MHCII-restricted CD4+ responses to gliomas. Our findings may have important clinical implications for the development of novel immunotherapeutic strategies targeting TREM2 and other myeloid-specific proteins in cancer treatment.

Discussion

In this study, we showed that depletion of TREM2 did not result in beneficial effects in our preclinical models of GBM. In addition to our utilization of the GL261 and 73C glioma models, another research group employed the CT2A brain tumor model and reported comparable findings.[40] Affirming our results, their investigation likewise demonstrated that TREM2-deficient mice did not exhibit prolonged survival but instead displayed a tendency toward shorter survival times. Moreover, our analysis revealed that nearly all tumor-microglia and macrophages exhibited high TREM2 expression in both patient GBM and mouse GL261 models. This finding suggests that the overall rise in TREM2 expression is likely connected to the significant influx of myeloid cell infiltration following tumor appearance. The increased TREM2 expression in glioma may not be the causal driver of tumor progression at least in the model of GL261, 73C, and CT2A.

Furthermore, our results implied that there are differences in tumor immunity between the brain and peripheral tissues. In preclinical models of colon carcinoma and melanoma, CD8+ T cells have been shown to be the primary mediators of tumor reduction, and their depletion has been found to eliminate the protective benefits of both genetic and immunotherapeutic interventions.[46,47] Additionally, in metastatic melanoma patients who responded to PD-1 blockade treatment, tumor regression was accompanied by the proliferation of CD8+ T cells.[48] In this paradigm, TREM2 deficiency reduced the immunosuppressive activity of myeloid cells, which in turn led to improved preservation and functionality of CD8+ T cells responding to anti-PD-1; as a result, overall survival in mice was improved in *Trem2*$^{-/-}$ compared with WT mice.[3,4,21,22] However, anti-PD-1/PD-L1 immunotherapy has shown limited efficacy in most clinical studies of GBM.[49] CD4+ T cells not only provide essential help to B cells for effective antibody-mediated immune responses.[50,51] Preclinical models of glioma, such as GL261 and 005 GSC, have demonstrated that CD4+ T cells are essential for tumor clearance and can induce tumor regression through therapeutic interventions without requiring CD8+ T cells.[5,6,52,53]

It is noteworthy that the specific cell line utilized can substantially affect results. For instance, SB28 tumor clearance might lean more on CD8+ responses,[39] possibly due to the scarcity of neoantigens in SB28.[25] The presentation of neoantigens through MHCII is particularly important when CD4+ T-cell-mediated immune responses are more predominant.[1,42,54] In contrast, GL261 is known for its abundant neoantigens, potentially explaining the divergence in phenotype when compared to SB28. Nevertheless, in line with existing literature,[18,22] our current study showed that TREM2 deficiency reduces the number of MHCII+ macrophages and CD4+ T-cell infiltration in GL261 model. This may explain why we did not observe a significant beneficial effect, but unexpectedly the detrimental consequence of TREM2 deficiency in the preclinical models of GBM. In the CD4+ T-cell dominant context, the benefits of TREM2 deficiency on CD8+ T cells may still not outweigh the negative effects on CD4+ T cells.

We revealed that TREM2 deficiency impaired the ability of myeloid cells to uptake tumor debris, which is the first step in the antitumor response through the phagocytosis-MHCII antigen presentation-CD4+ axis (Figure 4K). This conclusion is drawn from both *in vivo* and *in vitro* assays. In the *in vivo* assay, we employed flow cytometry

to observe the red tumor signals within myeloid cells. Considering that *in vivo* phagocytosis might be influenced by tumor size, we established a more controlled environment by using BMDM, feeding them with apoptotic tumor cells instead of beads,[39] offering a precise and controlled approach to mimic physiological conditions. Our results are consistent with previous research in the CNS, where TREM2 is known to play a key role in the phagocytosis of apoptotic neurons.[13,55,56] In addition, TREM2 function in phagocytosis of protein aggregations has been increasingly recognized in neurodegenerative diseases.[57–59] Based on our findings, we reason that the impaired phagocytosis in TREM2 deficient mice may likely cause the reduced MHCII$^+$ macrophages in gliomas.

Additionally, our research provides insight into TREM2 expression beyond the myeloid population, as we identified a modest population of TREM2$^+$ T cells in both human GBM and murine GL261. This is especially noteworthy because TREM2 has recently been discovered as a sensor responsible for Th1 activation, and its deficiency in CD4$^+$ T cells impairs proinflammatory Th1 responses to infectious diseases.[60,61] Therefore, future studies using conditional TREM2 knockout will be required to dissect TREM2 functions in multiple tumor-associated immune cells.

In summary, we have demonstrated that TREM2 plays a protective role in gliomas through phagocytosis and antigen presentation. Furthermore, our findings emphasize the importance of evaluating both CD8$^+$ and CD4$^+$ responses in different tumor contexts when developing TREM2-targeted therapies. As TREM2 antagonists emerge as promising therapeutic targets for cancer treatment, it is crucial to fully understand the range of TREM2 functions in different immune cell types and scrutinize their impact on tumor progression.

Supplementary Material

Supplementary material is available online at *Neuro-Oncology* (https://academic.oup.com/neuro-oncology).

Keywords

glioma | TREM2 | tumor-associated macrophages

Acknowledgments

We express our gratitude to Dr. Marco Colonna (Washington University School of Medicine, St. Louis) for generously providing the TREM2 knockout mouse strain. We thank the all members of Wu lab at May for the discussions.

Conflict of interest statement

None declared.

Funding

This work was supported by the National Institutes of Health R35NS132326 (L-J.W.), K99NS1177992 (K.A.), R01NS122174 (A.J.J.), Mayo Clinic Cancer Center and Mayo Clinic Center for Biomedical Discovery (L-J.W.).

Authorship Statement

Conceptualization: J.Z. and L-J.W.; Investigation: J.Z., L.W., S.Z., W.Z., Y.C., D.B.B., T.H., A.D., S.G., S.X., R.A., and M.X.; Assisted in data analysis: K.A., and F.Q.; Writing: J.Z. and L-J.W.; Review and editing: D.B.B., H.D., A.J.J., A.Q-H., and L-J.W.; Funding acquisition: L-J.W.

Data Availability

Data available upon request to corresponding author.

Affiliations

Department of Neurology, Mayo Clinic, Rochester, Minnesota, USA (J.Z., L.W., S.Z., Y.C., D.B.B., A.D., S.X., F.Q., M.X., L-J.W.); Mayo Clinic Graduate School of Biomedical Sciences, Rochester, Minnesota, USA (J.Z., L.W., S.Z., W.Z., S.G., R.A-K.); Department of Immunology, Mayo Clinic, Rochester, Minnesota, USA (T.H., K.A., A.J.J., H.D., L-J.W.); Department of Neurologic Surgery, Mayo Clinic, Jacksonville, Florida, USA (R.A-K., A.Q-H.); Department of Neuroscience, Mayo Clinic, Jacksonville, Florida, USA (L-J.W.)

References

1. Alspach E, Lussier DM, Miceli AP, et al. MHC-II neoantigens shape tumour immunity and response to immunotherapy. *Nature*. 2019;574(7780):696–701.
2. Oh J, Magnuson A, Benoist C, Pittet MJ, Weissleder R. Age-related tumor growth in mice is related to integrin alpha 4 in CD8+ T cells. *JCI Insight*. 2018;3(21):e122961.
3. Molgora M, Esaulova E, Vermi W, et al. TREM2 modulation remodels the tumor myeloid landscape enhancing anti-PD-1 immunotherapy. *Cell*. 2020;182(4):886–900.e17.
4. Binnewies M, Pollack JL, Rudolph J, et al. Targeting TREM2 on tumor-associated macrophages enhances immunotherapy. *Cell Rep*. 2021;37(3):109844.
5. Chen D, Varanasi SK, Hara T, et al. CTLA-4 blockade induces CD4(+) T cell IFNgamma-driven microglial phagocytosis and anti-tumor function in glioblastoma. *Immunity*. 2023;56(9):2086.e8–2104.e8.
6. Kilian M, Sheinin R, Tan CL, et al. MHC class II-restricted antigen presentation is required to prevent dysfunction of cytotoxic T cells by

blood-borne myeloids in brain tumors. *Cancer Cell.* 2022;41(2):235–251.e9.
7. Unanue ER. Perspective on antigen processing and presentation. *Immunol Rev.* 2002;185(1):86–102.
8. Colonna M, Wang Y. TREM2 variants: new keys to decipher Alzheimer disease pathogenesis. *Nat Rev Neurosci.* 2016;17(4):201–207.
9. Do TH, Ma F, Andrade PR, et al. TREM2 macrophages induced by human lipids drive inflammation in acne lesions. *Sci Immunol.* 2022;7(73):eabo2787.
10. Bouchon A, Hernandez-Munain C, Cella M, Colonna M. A DAP12-mediated pathway regulates expression of CC chemokine receptor 7 and maturation of human dendritic cells. *J Exp Med.* 2001;194(8):1111–1122.
11. Ulland TK, Colonna M. TREM2 - a key player in microglial biology and Alzheimer disease. *Nat Rev Neurol.* 2018;14(11):667–675.
12. N'Diaye EN, Branda CS, Branda SS, et al. TREM-2 (triggering receptor expressed on myeloid cells 2) is a phagocytic receptor for bacteria. *J Cell Biol.* 2009;184(2):215–223.
13. Takahashi K, Rochford CD, Neumann H. Clearance of apoptotic neurons without inflammation by microglial triggering receptor expressed on myeloid cells-2. *J Exp Med.* 2005;201(4):647–657.
14. Wang Y, Cella M, Mallinson K, et al. TREM2 lipid sensing sustains the microglial response in an Alzheimer's disease model. *Cell.* 2015;160(6):1061–1071.
15. Zhao Y, Wu X, Li X, et al. TREM2 Is a Receptor for beta-amyloid that mediates microglial function. *Neuron.* 2018;97(5):1023–1031.e7.
16. Wang Y, Ulland TK, Ulrich JD, et al. TREM2-mediated early microglial response limits diffusion and toxicity of amyloid plaques. *J Exp Med.* 2016;213(5):667–675.
17. Xie M, Liu YU, Zhao S, et al. TREM2 interacts with TDP-43 and mediates microglial neuroprotection against TDP-43-related neurodegeneration. *Nat Neurosci.* 2022;25(1):26–38.
18. Cantoni C, Bollman B, Licastro D, et al. TREM2 regulates microglial cell activation in response to demyelination in vivo. *Acta Neuropathol.* 2015;129(3):429–447.
19. Scott-Hewitt N, Perrucci F, Morini R, et al. Local externalization of phosphatidylserine mediates developmental synaptic pruning by microglia. *EMBO J.* 2020;39(16):e105380.
20. Zhai K, Huang Z, Huang Q, et al. Pharmacological inhibition of BACE1 suppresses glioblastoma growth by stimulating macrophage phagocytosis of tumor cells. *Nat Cancer.* 2021;2(11):1136–1151.
21. Katzenelenbogen Y, Sheban F, Yalin A, et al. Coupled scRNA-seq and intracellular protein activity reveal an immunosuppressive role of TREM2 in cancer. *Cell.* 2020;182(4):872–885.e19.
22. Timperi E, Gueguen P, Molgora M, et al. Lipid-associated macrophages are induced by cancer-associated fibroblasts and mediate immune suppression in breast cancer. *Cancer Res.* 2022;82(18):3291–3306.
23. Zhang H, Liu Z, Wen H, et al. Immunosuppressive TREM2(+) macrophages are associated with undesirable prognosis and responses to anti-PD-1 immunotherapy in non-small cell lung cancer. *Cancer Immunol Immunother.* 2022;71(10):2511–2522.
24. Haddad AF, Young JS, Amara D, et al. Mouse models of glioblastoma for the evaluation of novel therapeutic strategies. *Neuro-Oncol Adv.* 2021;3(1):vdab100.
25. Letchuman V, Ampie L, Shah AH, et al. Syngeneic murine glioblastoma models: reactionary immune changes and immunotherapy intervention outcomes. *Neurosurg Focus.* 2022;52(2):E5.
26. Singh DK, Kollipara RK, Vemireddy V, et al. Oncogenes activate an autonomous transcriptional regulatory circuit that drives glioblastoma. *Cell Rep.* 2017;18(4):961–976.
27. Gao X, Zhang Z, Mashimo T, et al. Gliomas interact with non-glioma brain cells via extracellular vesicles. *Cell Rep.* 2020;30(8):2489–2500.e5.
28. Corbett TH, Griswold DP, Jr, Roberts BJ, Peckham JC, Schabel FM, Jr. Tumor induction relationships in development of transplantable cancers of the colon in mice for chemotherapy assays, with a note on carcinogen structure. *Cancer Res.* 1975;35(9):2434–2439.
29. Ayasoufi K, Pfaller CK, Evgin L, et al. Brain cancer induces systemic immunosuppression through release of non-steroid soluble mediators. *Brain.* 2020;143(12):3629–3652.
30. Pombo Antunes AR, Scheyltjens I, Lodi F, et al. Single-cell profiling of myeloid cells in glioblastoma across species and disease stage reveals macrophage competition and specialization. *Nat Neurosci.* 2021;24(4):595–610.
31. Hao Y, Hao S, Andersen-Nissen E, et al. Integrated analysis of multimodal single-cell data. *Cell.* 2021;184(13):3573–3587.e29.
32. Korsunsky I, Millard N, Fan J, et al. Fast, sensitive and accurate integration of single-cell data with Harmony. *Nat Methods.* 2019;16(12):1289–1296.
33. Andreatta M, Corria-Osorio J, Muller S, et al. Interpretation of T cell states from single-cell transcriptomics data using reference atlases. *Nat Commun.* 2021;12(1):2965.
34. Cumba Garcia LM, Huseby Kelcher AM, Malo CS, Johnson AJ. Superior isolation of antigen-specific brain infiltrating T cells using manual homogenization technique. *J Immunol Methods.* 2016;439:23–28.
35. Liu YU, Ying Y, Li Y, et al. Neuronal network activity controls microglial process surveillance in awake mice via norepinephrine signaling. *Nat Neurosci.* 2019;22(11):1771–1781.
36. Eyo UB, Mo M, Yi MH, et al. P2Y12R-Dependent translocation mechanisms gate the changing microglial landscape. *Cell Reports.* 2018;23(4):959–966.
37. Tang Z, Li C, Kang B, et al. GEPIA: a web server for cancer and normal gene expression profiling and interactive analyses. *Nucleic Acids Res.* 2017;45(W1):W98–W102.
38. Klemm F, Maas RR, Bowman RL, et al. Interrogation of the microenvironmental landscape in brain tumors reveals disease-specific alterations of immune cells. *Cell.* 2020;181(7):1643.e17–1660.e17.
39. Sun R, Han R, McCornack C, et al. TREM2 inhibition triggers antitumor cell activity of myeloid cells in glioblastoma. *Sci Adv.* 2023;9(19):eade3559.
40. Peshoff MM, Gupta P, Trivedi R, et al. Triggering receptor expressed on myeloid cells 2 (TREM2) regulates phagocytosis in glioblastoma. *bioRxiv.* 2023:2005.
41. Hill RA, Damisah EC, Chen F, Kwan AC, Grutzendler J. Targeted two-photon chemical apoptotic ablation of defined cell types in vivo. *Nat Commun.* 2017;8:15837.
42. Kruse B, Buzzai AC, Shridhar N, et al. CD4(+) T cell-induced inflammatory cell death controls immune-evasive tumours. *Nature.* 2023;618(7967):1033–1040.
43. Stock AD, Der E, Gelb S, et al. Tertiary lymphoid structures in the choroid plexus in neuropsychiatric lupus. *JCI Insight.* 2019;4(11):e124203.
44. Beltra JC, Manne S, Abdel-Hakeem MS, et al. Developmental relationships of four exhausted CD8(+) T cell subsets reveals underlying transcriptional and epigenetic landscape control mechanisms. *Immunity.* 2020;52(5):825–841.e8.
45. Duhen R, Fesneau O, Samson KA, et al. PD-1 and ICOS coexpression identifies tumor-reactive CD4+ T cells in human solid tumors. *J Clin Invest.* 2022;132(12):e156821.
46. Katkeviciute E, Hering L, Montalban-Arques A, et al. Protein tyrosine phosphatase nonreceptor type 2 controls colorectal cancer development. *J Clin Invest.* 2021;131(1):e140281.
47. Ji S, Lee J, Lee ES, Kim DH, Sin JI. B16 melanoma control by anti-PD-L1 requires CD8+ T cells and NK cells: application of anti-PD-L1 Abs and Trp2 peptide vaccines. *Hum Vaccin Immunother.* 2021;17(7):1910–1922.

48. Tumeh PC, Harview CL, Yearley JH, et al. PD-1 blockade induces responses by inhibiting adaptive immune resistance. *Nature*. 2014;515(7528):568–571.
49. Yang T, Kong Z, Ma W. PD-1/PD-L1 immune checkpoint inhibitors in glioblastoma: clinical studies, challenges and potential. *Hum Vaccin Immunother*. 2021;17(2):546–553.
50. Eisenbarth SC, Baumjohann D, Craft J, et al. CD4(+) T cells that help B cells - a proposal for uniform nomenclature. *Trends Immunol*. 2021;42(8):658–669.
51. Gutierrez-Melo N, Baumjohann D. T follicular helper cells in cancer. *Trends Cancer*. 2023;9(4):309–325.
52. Murphy KA, Erickson JR, Johnson CS, et al. CD8+ T cell-independent tumor regression induced by Fc-OX40L and therapeutic vaccination in a mouse model of glioma. *J Immunol*. 2014;192(1):224–233.
53. Murphy KA, Griffith TS. CD8 T cell-independent antitumor response and its potential for treatment of malignant gliomas. *Cancers*. 2016;8(8):71.
54. Speiser DE, Chijioke O, Schaeuble K, Munz C. CD4(+) T cells in cancer. *Nat Cancer*. 2023;4(3):317–329.
55. Kawabori M, Kacimi R, Kauppinen T, et al. Triggering receptor expressed on myeloid cells 2 (TREM2) deficiency attenuates phagocytic activities of microglia and exacerbates ischemic damage in experimental stroke. *J Neurosci*. 2015;35(8):3384–3396.
56. Atagi Y, Liu CC, Painter MM, et al. Apolipoprotein E is a ligand for triggering receptor expressed on myeloid cells 2 (TREM2). *J Biol Chem*. 2015;290(43):26043–26050.
57. Xie M, Zhao S, Bosco DB, Nguyen A, Wu LJ. Microglial TREM2 in amyotrophic lateral sclerosis. *Dev Neurobiol*. 2022;82(1):125–137.
58. Zhao N, Bu G. A TREM2 antibody energizes microglia. *Nat Neurosci*. 2023;26(3):366–368.
59. Colonna M. The biology of TREM receptors. *Nat Rev Immunol*. 2023;23(9):580–594.
60. Wu Y, Wu M, Ming S, et al. TREM-2 promotes Th1 responses by interacting with the CD3zeta-ZAP70 complex following Mycobacterium tuberculosis infection. *J Clin Invest*. 2021;131(17):e137407.
61. Wu Y, Wang M, Yin H, et al. TREM-2 is a sensor and activator of T cell response in SARS-CoV-2 infection. *Sci Adv*. 2021;7(50):eabi6802.